Molecular Dynamics Study of Water Interacting with Siloxane Surface Modified by Poly(ethylene oxide) Chains

ARTICLE *in* THE JOURNAL OF PHYSICAL CHEMISTRY C · SEPTEMBER 2011

Impact Factor: 4.77 · DOI: 10.1021/jp205973h

2 AUTHORS:

Zuzana Benková
Slovak Academy of Sciences
23 PUBLICATIONS **359** CITATIONS
SEE PROFILE

Natália D. S. Cordeiro
University of Porto
245 PUBLICATIONS **3,049** CITATIONS
SEE PROFILE

THE JOURNAL OF PHYSICAL CHEMISTRY C

Article

pubs.acs.org/JPCC

Molecular Dynamics Study of Poly(Ethylene Oxide) Chains Densely Grafted on Siloxane Surface in Dry Conditions

Zuzana Benková*[,†,‡] and M. Natália D. S. Cordeiro*[,†]

[†]REQUIMTE, Department of Chemistry, University of Porto, Rua do Campo Alegre 687, 4168-007 Porto, Portugal

[‡]Polymer Institute, Slovak Academy of Sciences, Dúbravská cesta 9, 845 41 Bratislava, Slovakia

Supporting Information

ABSTRACT: In this work, we present results of a molecular dynamics study of poly(ethylene oxide) (PEO) chains of varying length N covalently end-grafted to a strongly attractive siloxane surface in dry conditions. The investigated coverage densities σ span a wide interval ranging from sparse to very dense coating of the siloxane plane. Our results show that no phase separated clusters are observed because of the strong affinity of ethylene oxide monomers for the siloxane surface. Upon dehydration, the dry systems become contracted and compacted. The monomer and chain-end density distributions are in qualitative accord with theoretical predictions. The brush height scales linearly with N and σ. The organization of monomers at lower coverage densities is controlled by the attractive interactions with the siloxane support giving rise to an anisotropically collapsed conformation of PEO layer. The highest coverage densities are responsible for the alignment of chains in perpendicular directions with a nematic liquid-like ordering. The balance between the attraction invoked by the siloxane surface and the lateral repulsion at higher σ seems to appear at σ = 2.185 nm^{-2}.

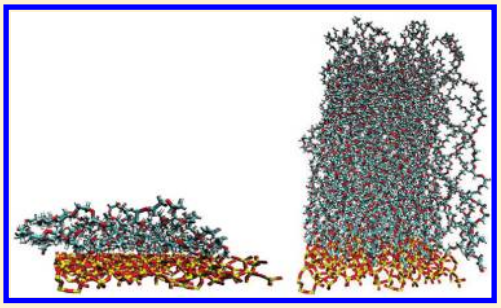

1. INTRODUCTION

Polymers chemically or physically tethered at one of their ends to a solid substrate have attracted a great deal of interest from the scientific community in the last years. This stems mainly from their wide variety of functions and applications in biological, chemical, or technological processes. Actually, the static and dynamic properties of polymer chains grafted onto some interface differ significantly from those of the free-chain counterparts. In solution, depending on the coverage surface density of the attached chains, at least two conformational regimes might be recognized. In the low density regime, the chains are separated sufficiently and mutually do not overlap. In the case of absent attractive interactions between these macromolecules and the impenetrable interface, the chains adopt coiled half-spaced conformation similar to the conformation of free unperturbed chains in the same conditions. This low-coverage density regime is known as the mushroom regime. The alternative pancake regime emerges if the nonoverlapped chains are adsorbed onto the supporting substrate, thus forming two-dimensional structures. As the coverage density exceeds $\sim 1/(\pi R_g^2)$, where R_g is the radius of gyration of the corresponding free unperturbed chain, the chains are exposed to lateral interactions with monomers of adjacent chains, and in order to release the energy penalty due to this crowding, they are expanded in a vertical direction away from the substrate. The layer of such extended end-grafted chains refers to the polymer brush.

The transition between the low- and high-coverage density regimes is not a step-like process for grafted chains of intermediate molecular weight. However, plenty of experimental studies have been carried out on chains of intermediate contour length and thus far from the long chain limit for which the analytical theory is well elaborated.[1−3]

The driving force for chain stretching in the vertical direction from the supporting material is the excess potential energy arising from the lateral repulsion of overcrowded densely packed chains. The overlaying chains are expanded away from the grafting support, and their ensuing conformations are ruled by the compromise between the loss of interaction potential energy and elastic entropy.

Objects modified by coating with polymer brushes also exhibit altered mechanical or chemical properties, for instance, enhanced inertness and resistance to protein adsorption or platelet adhesion.[4] Polymer brushes have important biological and technological applications ranging from lubrication[5] through colloid stabilization[6] to inhibition of deposition on surfaces.[7,8]

The height of the brush depends on the coverage density σ, the length of grafted chains N, and the solvent quality. According to the scaling approach of Alexander[9] and congruent results achieved by the Flory-type arguments of de Gennes,[10] the height h of a brush in good-solvent conditions scales as $h \sim N\sigma^{1/3}$. The SCF theory,[1−3] based on the presumption of sufficiently high coverage density, allowing then to apply Gaussian statistics to the description of the chain behavior, renders qualitatively the same scaling and differs only in a

Received: October 12, 2011
Revised: January 10, 2012
Published: January 13, 2012

numerical prefactor. However, the former approach[9,10] predicts that the density distribution of chain monomers in the direction perpendicular to the grafting plane is represented by a uniform step function steeply decaying to zero at the brush height and that the free terminal monomers are strictly located at the frontal edge of the brush layer. On the opposite, SCF theory[1−3] provides the parabolic monomer-density dependence on the distance from the grafting surface, which vanishes at the brush height. The free ends of grafted polymers are distributed everywhere in the brush with a linear initial increase of probability, faster decay after maximum at $h/2^{1/2}$ and zero value at h. Apart from the high coverage density (but not too high for neglecting three-body interaction terms), another limitation of the SCF analysis rests in considering infinitely long chains and no specific interactions between the components constituting brush systems.

Simple concepts based on the blobs of size $\sigma^{-1/2}$ yield a general scaling relationship for the thickness of brush layer, that is, $h \sim N\sigma^{(1-\upsilon)/2\upsilon}$ with exponents υ = 3/5, 1/2, and 1/3, respectively, in good-, theta-, and poor-solvent conditions. For dry brush systems, i.e., chains anchored at an interface with air, the air is considered as the poor solvent, and thus, the scaling should be linear in both N and σ. Anyway, when comparing the linear dependence on molecular weight of the brush height in solvents of all qualities (a function of N) to the corresponding free chain dimensions, the expansion of the tethered chains is apparent.

The real systems exhibit more complex conformations arising from the specific interactions, which are usually not accounted for in the theoretical derivations. However, molecular simulations can capture also the specific interactions encountered in brush systems and complementary to the analytical methods can be used for not too long polymers. Simulation methods including molecular dynamics (MD),[11−13] Monte Carlo (MC),[14−17] dissipative particle dynamics (DPD),[18] Brownian dynamics (BD)[19] are frequently employed and may potentially support experimental techniques dealing with the brush systems such as surface force apparatus,[20] small angle neutron scattering,[21] neutron reflectivity,[22] and X-ray photoelectron spectroscopy.[23] Yet, because the coarse-grained approach dominates most of the applied simulation methods, the atomistic details needed for the description of specific interactions are usually lost. Indeed, there is only a scarce number of computer simulation studies dealing with the brush systems represented at the atomistic level[24−27] out of which only one study deals with dry brushes.[25]

Poly(ethylene oxide) (PEO) belongs to the most widespread polymers used in plenty of areas. Thanks to its amphiphilic nature, it is perfectly soluble in water and other hydrophilic as well as hydrophobic solvents. Since PEO is generally considered to be a very good protein-resistant agent and along with its biocompatibility, biological inertness, low immunogenicity and toxicity, it has gained increased biomedical application as a coating material, which protects surfaces and membranes against protein adsorption.[28,29]

The great number of experimental studies on grafted PEO polymers prompted us to simulate these systems using MD method on all-atom basis and to fill thus the gap in the field of atomistic studies. In the experimental setups, very often the silica[30] or glass layers[31] constitute the underlying substrates for PEO; therefore, we have also assumed the amorphous siloxane as the surface irreversibly supporting the PEO chains. Notice that the hydration effects on PEO chains terminally tethered to the siloxane surface have already been investigated by us recently.[32]

The present study is focused on the equilibrium structural properties of layers composed of dry PEO chains covalently attached to the siloxane surface. The dry layers of anchored chains are relevant in technology as stabilizing coating films[33] or protecting agents[34] and experimental measurements are frequently conducted on these systems.[35] Systems of dry PEO brushes in which a PEO chain was restricted to an area as small as about 0.25 nm^2 have been examined, being thus the respective packing of these chains even tighter than in the crystalline phase where the shortest separation is 0.656 nm.[36] Such coverage densities exceed the upper limit of coverage densities experimentally attainable so far.[31,37] Properties such as monomer density distributions, distributions of the free terminal monomers as functions of the distance from the siloxane surface, were calculated and compared with their hydrated counterparts. The organization of monomers within the PEO layer is aimed as well. The low-density and high-density regimes were examined more thoroughly also due to the potential formation of phase separated clusters and a nematically collapsed phase, respectively. Using an atomistic model such as the one used here rather than the coarse-grained models represents a more realistic system and thus seems to be a suitable bridge between the analytical predictions and experimental findings. Moreover, the majority of theoretical and simulation studies, with a few exceptions,[16] dealing with the irreversibly grafted macromolecules, have assumed purely repulsive interactions with the grafting support. but in the presented systems, the interactions between PEO chains and siloxane atoms do not exclude attractions.

The rest of this article is organized as follows. The systems' molecular models, the potential functions, and the details of the simulations are outlined in the next section. Section 3 presents the results obtained in this study. In section 4, a picture of the properties of our polymeric systems is drawn, based on the results reported in previous sections, and our main conclusions are summarized.

2. METHODOLOGY

The systems composed of PEO chains attached to an amorphous siloxane substrate (silica without free OH groups) at one end, terminated by methyl group at the other end were simulated using the MD method. PEO chains comprised N = 18, 24, and 30 oxygen atoms with the last one harmonically bonded to a silicon atom. Symbol N identifies the number of monomers throughout the article. The coverage density σ of grafted PEO chains, expressed as the number of chains attached to a unit area, ranged between 0.437 and 3.932 nm^{-2}. The starting conformations of the systems were designed as stretched, rod-like PEO chains with the helical axis vertically oriented to the siloxane plane. The normal of the siloxane plane (xy) is the z axis in the Cartesian coordinate system throughout this study. The atoms of the amorphous siloxane surface were kept frozen during the MD simulations and participated only in nonbonded interactions with the atoms of PEO chains and water. The thickness of the siloxane layer was 0.8 nm, which was enough to account for all relevant nonbonded interactions between the PEO chains and siloxane atoms. Here, it should be remarked that a too thin solid layer would underestimate the attractive interactions. All MD simulations were performed using the GROMACS package.[38,39] The all-atom intra- and intermolecular interactions were described by the revised

dx.doi.org/10.1021/jp209802p | J. Phys. Chem. C 2012, 116, 3576−3584

CHARMM force field.[40,41] The Lennard-Jones parameters used for silicon and oxygen atoms within the siloxane layer are compatible with the CHARMM force field.[42] Since the periodic boundary conditions were applied in all dimensions, the heights as well as the sides of square based simulation boxes were set sufficiently long (4.279 nm × 4.279 nm × 15.0 nm) to prevent interactions between a given particle and its periodic images in all directions.

First, the systems were simulated in semi-isotropic *NPT* ensemble (P = 1 bar; T = 298 K) for 100 ps using the Parrinello−Rahman barostat[43,44] with a relaxation time of 0.5 ps. During this stage of simulations, all bonded parameters were fully unconstrained, in order to adjust correctly the bond lengths, and the time step was set to 1 fs. The final conformations from these constant-surface-pressure runs were then used as input structures for *NVT* ensemble simulations at 400 K. On these *NVT* simulations, the temperature was kept fixed by applying the Nosé−Hoover thermostat[45,46] and resorting to a relaxation time of 0.1 ps. After an initial run of 10 ns at 400 K, the temperature was gradually dropped-down to 300 K during the time interval of 1 ns. Then, the simulations were continued in the *NVT* ensemble at 298 K with a time step of 2 fs and constraining all bond lengths using the LINCS algorithm.[47] After an equilibration period of 10 ns, averaging was carried out over all chains on a trajectory length of 20 ns. The time interval between sampling conformations was 5 ps. The relaxation times extracted from the autocorrelation functions of the end-to-end distance and radius of gyration for grafted PEO chains were for all chain lengths less than 4 ns. The particle-mesh Ewald method,[48,49] with a real space cutoff of 1.4 nm, including a correction term suggested by Yeh and Berkowitz for systems with a slab geometry,[50] was applied to handle the long-range electrostatic interactions. The Lennard-Jones (L-J) potential was smoothly shifted to zero between 1.0 and 1.2 nm. Both the real-space part of the Ewald summation and the short-range L-J interactions were calculated within a radius of 1.4 nm with help of a neighbor list updated every 10 time steps. Full details of the simulation setups are given in the Supporting Information.

3. RESULTS AND DISCUSSION

3.1. Monomer Density Distributions. The performed simulations of single free PEO chains of N = 18, 24, and 30 monomers with their initial stretched helical conformations aligned horizontally with the siloxane surface have shown that the siloxane substrate attracts the short PEO chains so strongly that the two shorter chains are even prevented from relaxation, and only the chain of N = 30 slightly curls up forming a two-dimensional structure. As the snapshots in Figure 1 illustrate, the expansion of PEO chains away from the siloxane support is achievable by swelling chains in the good solvent (Figure 1b) or decreasing interchain separation (Figure 1c). We have carried out as well simulations of the sparsely covered siloxane surface (σ = 0.055 and 0.218 nm^{-2}). Instead of the monomer phase aggregation reported by coarse-grained simulations and experimental investigation for shorter chains grafted at lover coverage densities,[12,35,51] the PEO chains are completely adsorbed at the siloxane surface. The instantaneous vacant spaces are randomly distributed and thus result from the paucity of ethylene oxide (EO) monomers rather than from the formation of three-dimensional clusters. In order to prove this assertion, we have simulated also systems of nonoverlapping PEO chains grafted on a predominantly repulsive substrate

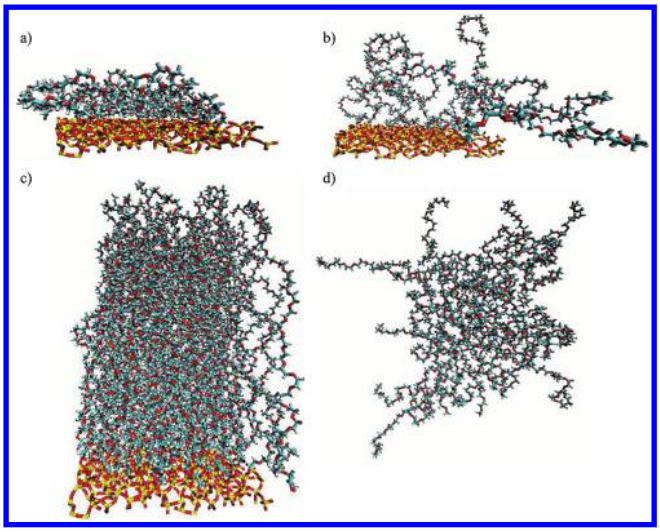

Figure 1. Snapshots displaying side views of PEO chains of length N = 30 grafted on the siloxane surface at σ = 0.437 nm^{-2} in dry conditions (a), at σ = 0.437 nm^{-2} in water (water molecules have been removed for the sake of clarity) (b), and at σ = 3.932 nm^{-2} in dry conditions (c). The top view of the aggregated PEO chains of N = 30 grafted at σ = 0.218 nm^{-2} on a repulsive substrate is also included; the siloxane surface has been omitted in this case (d).

(modeled by surface atomic radius increased to 0.9 nm and surface L-J interaction energy reduced to 0.001 kJ·mol^{-1}). Table S1 in the Supporting Information provides a complete list of the nonbonded interaction parameters used in this work. In that case, aggregates of mutually interpenetrating PEO chains are clearly observed (Figure 1d). To the best of our knowledge, the effect of attractive interactions between the grafted chains and grafting support has been addressed so far neither at the coarse-grain nor at the atomistic level.

The nonoverlapping PEO chains are prone to adopt pancake-like conformation as it is clear from the scaling of the radius of gyration with the number of monomers N^{ν}, where $\nu > 3/5$ (Figure S1, Supporting Information). In all studied systems of overlapping chains, the interaction energy per one monomer (in absolute values) develops linearly with the coverage density and does not depend on the chain length (Figure S2, Supporting Information).

The monomer density distribution ρ along the z axis (z = 0 corresponds to the averaged position of the siloxane oxygen atoms forming only one Si−O bond) reduced by the coverage density σ is shown in Figure 2 for the PEO chains of length N = 30 grafted at the coverage densities, which for the hydrated PEO chains, meet criteria of the brush regime (i.e., a flat region in the monomer density distributions and scaling of the brush height with the coverage density).[32] The first and the second peaks in these distributions are found at about 0.3 and 0.6 nm, respectively, regardless of the presence or absence of water; however, water molecules at the siloxane interface are responsible for reduction of their intensities.[32,52] The distributions of the grafted PEO chains in dry conditions display an oscillating behavior also further away from the siloxane surface with gradually attenuating amplitudes. However, as it is evident from the plateau region in the density distributions for hydrated PEO chains, water swells the chains more and consequently damps the PEO density in the brush layer. This is in line with the SCF theory, which assumes that the brush height increases with the solvent quality. The initial

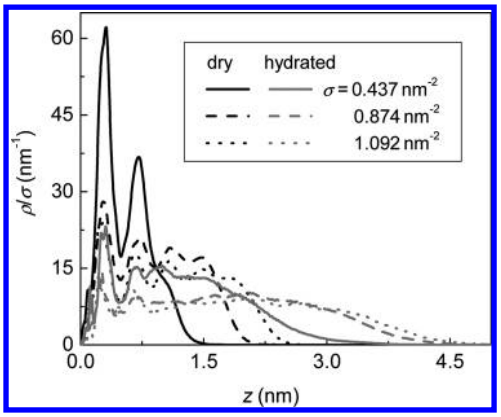

Figure 2. Monomer density distribution reduced by the respective coverage density as a function of the distance from the siloxane surface for PEO chains of N = 30 in dry (black lines) and hydrated (gray lines) conditions grafted at coverage densities σ.

depletion zone, not predicted by the SCF theory,[1−3] is slightly narrowed in the dry, not too densely covered siloxane surfaces. The probability of finding a monomer adsorbed directly on the siloxane surface is nonzero, which is a consequence of the attractive interactions between the EO monomers and siloxane atoms. A vanishing probability at the end occurs more abruptly for the dry analogues. This is caused by the reorganization of free terminal atoms to the periphery of the PEO layer.

Figure 3 displays the monomer density distributions for dry PEO layers grafted at higher σ. These distributions are

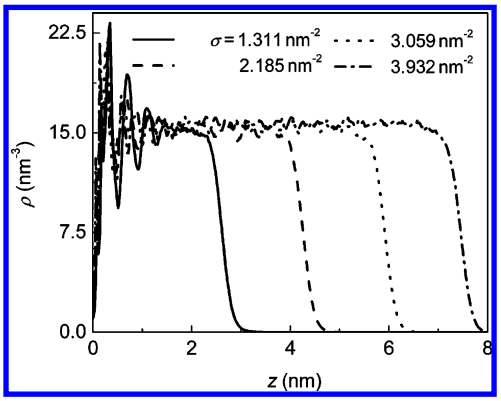

Figure 3. Monomer density distribution as a function of the distance from the siloxane surface for dry brushes composed of PEO chains of N = 30 monomer and grafted at coverage densities σ.

becoming more step-like, which agrees with the mean-field predictions elaborated for the collapsed brush layers.[53] Nevertheless, the considerable oscillations and the depletion region are in contrast with the theoretical analyses that render the flat monomer distribution governed only by the second and third virial coefficients.[53] The oscillations in the density distributions most likely follow from the closely packed chain structures at higher coverage densities. The crossover to the brush regime is not steep however, being the plateau in the monomer density distributions a sign of the brush regime. For investigated systems, the onset of plateau formation is observed at about 1.748 nm^{-2} for N = 18 and 24 and at about 1.092 nm^{-2} for N = 30.

Since even according to the simple scaling analyzes, based on the blob model, the brush height evolves linearly with the number of monomers constituting the grafted chains, the abruptly ceasing tails of the monomer density distribution for the coverage densities, where the plateau region is well developed, are plotted in Figure 4 against the z abscissa

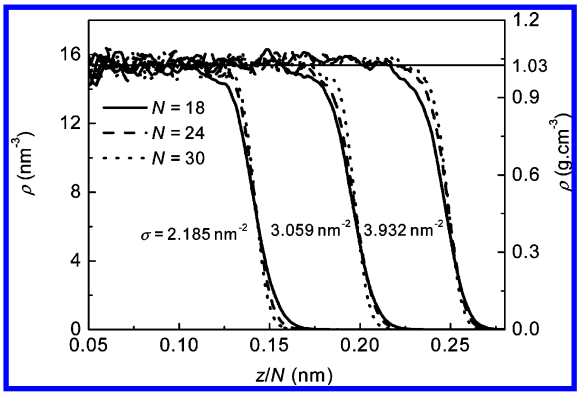

Figure 4. Monomer density distribution as a function of the distance from the siloxane surface reduced by the number of monomers for layers built up of PEO chains of N = 18, 24, and 30 monomers grafted at the indicated coverage densities σ. The solid horizontal line designates the average value (1.03 g·cm^{-3}) of monomer density in the plateau region.

reduced by the different number of monomers N = 18, 24, and 30. For a given coverage density, the curves are getting closer but the coalescence is not very satisfactory. This inconsistency can be ascribed to the short chain lengths N. For longer PEO chains, the distributions tend to vanish faster. The relatively weaker stretching of chains at their end manifests itself by an inflection point followed by the convex fall-down. Such a pattern is typical for the simulated systems.[12,14,25] The width of the plateau correlates with the brush height and the value of monomer density oscillates in this region around the value of 1.03 g·cm^{-3} and more for longer chains, which is close to our estimate for bulk free PEO chains obtained in *NPT* ensemble, the later being about 1.11−1.12 g·cm^{-3}. Here, it should be referred that the reported experimental density of PEO melt is 1.13 g·cm^{-3}.[54]

3.2. Density Distributions of Free Chain Ends. Another intriguing feature identifying polymer brushes is the probability of finding free chain ends in the space above the grafting support. The density distributions of free chain ends ρ_e along the z axis for the dry layers built up of grafted PEO chains of N = 30 monomers are compared with their hydrated analogues in Figure 5 for σ = 0.437 and 1.092 nm^{-2}, that is to say, the coverage densities conforming to the onset of the brush regime for hydrated[32] and dry PEO layers, respectively. As it is clear from Figure 5, the free terminal atoms of the dry PEO chains are found also at the siloxane surface, in contrast with the hydrated PEO layers. The occurrence of the hydrated terminal atoms is more diffusive and extended further away from the siloxane surface.

As Figure 6 clearly shows, scaling of z axis by the monomer number leads to a collapse of the tailing parts in the chain-end distributions for the larger coverage densities. The multimodal character dominating the chain-end density distributions for the lower σ values is suppressed by increasing σ. The peaks at lower distances z are transformed to a plateau preceding the single peak, which is narrowed upon increasing coverage density, once the coverage density surpasses 1.092 nm^{-2}. Surprisingly, at the higher coverage densities, the density distributions for the

dx.doi.org/10.1021/jp209802p | J. Phys. Chem. C 2012, 116, 3576−3584

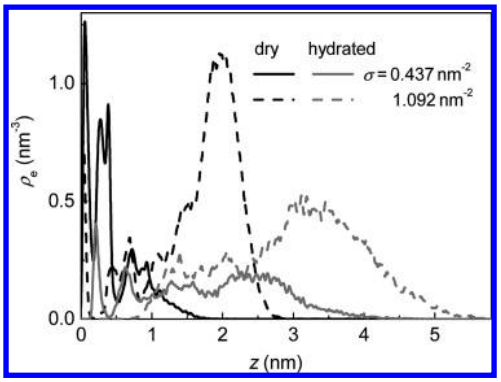

Figure 5. Density distribution of the free terminal PEO atoms as a function of their distance from the siloxane surface for PEO chains of $N = 30$ grafted at different coverage densities σ in the absence of water (black lines) and in the presence of water (gray lines).

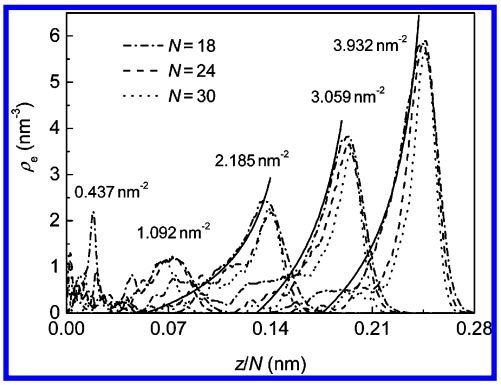

Figure 6. Density distribution of the free terminal PEO monomers as a function of their scaled distance from the siloxane surface for PEO chains of N monomers grafted at indicated coverage densities σ. The solid lines illustrate the mean-field predictions shifted along both axes to achieve the agreement with simulation plots as good as possible.

shorter chain lengths fit better the mean-field estimate (see the solid line in Figure 6 appropriately shifted along both axes) in poor-solvent conditions, given by $\propto z'(1 - z'^2)^{1/2}$ with $z' = z/N$.[53] The ends of longer PEO chains are expelled more to the periphery of the brush as can be recognized by the steeper turnover of their density distributions. Here, one should take into consideration also the attraction of the terminal monomers invoked by the siloxane surface, which is more efficiently shielded at PEO layers composed of longer chains. Thus, the improved agreement for the shorter chains appears to be just a coincidence.

3.3. Extension of PEO Layer Away from Siloxane Surface. The brush height h is quantified as the normalized first moment of the monomer density distribution function. Similarly, the averaged distance from the siloxane surface $h(i)$ of a monomer i (indexing within the chain backbone from the grafting monomer onward) is measured as the normalized first moment of the individual monomer density distribution functions.

Figure 7 provides the plots of the height of the PEO layer and the average distance of the chain ends from the siloxane surface in their reduced forms as functions of the coverage density in the logarithmic scale. The collapse of plots onto a single line for all three investigated chain lengths and for $\sigma > 1.092$ nm^{-2} pinpoints evidence for the linear dependence of the average height and terminal monomer distance from the

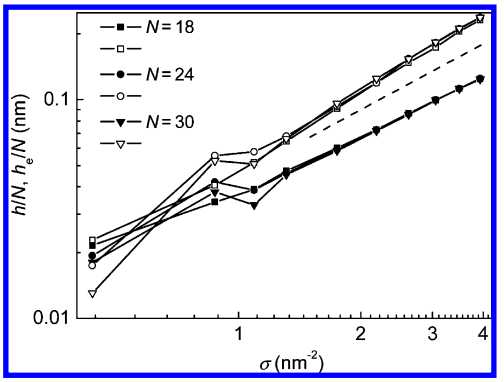

Figure 7. Average height of PEO layers (solid symbols) and average distance of the terminal backbone atoms from the siloxane surface (open symbols) reduced by the number of monomers plotted against the coverage density for grafted PEO chains of contour length N in the logarithmic scale. The dashed line with the slope of 1 is also displayed for comparison.

grafting plane on the chain length. As one can see in Figure 7, the slopes for presented realistic systems are close to the predicted value of 1, displayed by the dashed line. Plots of h/N and h_e/N are approaching this slope from the bottom (exponent $\approx$ 0.9) and top (exponent $\approx$ 1.13−1.15), respectively. The coalescence for the chain-end distance dependence is slightly less satisfactory. However, the extrapolated estimate of N for exponent of 1 is $N = 50$ for the chain-end distance. The departure of the three lowest points is most likely a consequence of the transition regime to the stretched brush conformations combined with the attractive effects of the siloxane surface more appreciable over the whole chain backbone at these coverage densities. At higher coverage densities, the PEO grafted chains are stretched substantially in spite of their attractive interactions with the siloxane surface. For instance, at $\sigma = 3.932$ nm^{-2}, the extension of chains attains about 75% of their entirely straightened zigzag conformation. These findings show that the theoretical predictions, which do not take into account the atomistic details and attractive interactions between a grafted chain and the supporting surface, are still applicable to dense polymer brushes that assume these aspects.

In order to get more detailed insight into the organization of individual monomers within the PEO grafted layer, the distance of the consecutive monomers from the siloxane surface is presented in Figure 8 as a function of the monomer index i in the form reduced by N, $h(i)/N = f(i/N)$, for all three chain lengths at different coverage densities. As expected from Figure 7, all curves perfectly collapse onto one single curve, especially for $\sigma > 1.092$ nm^{-2}. This implies that the degree of extension along the PEO contour length is determined by the absolute length of the backbone. Though, the curves possess different behavior.

It is clear that the plot for $\sigma = 0.437$ nm^{-2} only modestly increases, and after it reaches a low and broad peak, it slowly decreases. At this coverage density, the lateral crowding of chains is not so severe, and this promotes the monomers to collapse due to the absence of a solvent (poor-solvent conditions are supplied by the empty-volume space). Because of the strong affinity of the EO monomers for the siloxane supporting plane, the terminal monomers are allowed to intercalate somewhat deeper into the PEO layer as they are more flexible. The shape of the plots for the intermediate

dx.doi.org/10.1021/jp209802p | J. Phys. Chem. C 2012, 116, 3576−3584

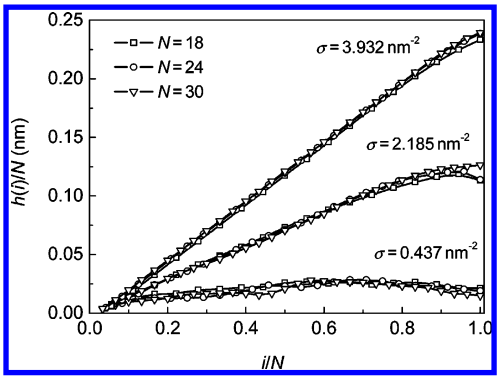

Figure 8. Average distance of the ith monomer $O-CH_2{}^*-CH_2$ (the asterisk assigns the reference atom) from the siloxane surface versus the contour position of the ith monomer for PEO chains of lengths N grafted at indicated coverage densities σ. Both axes are reduced by the number of monomers within a chain.

coverage density, σ = 2.185 nm^{-2}, is getting close to the sinusoidal shape, $\sin(i\pi/2N)$, predicted by the SCF theory for solvents of all qualities. Yet, there is a decline at the end for chains of N = 18 and 24. This small maximum originates from the more flexible terminal part of the chains due to the locally reduced monomer density at the outer region of the PEO brush. For the highest coverage densities, the dependence is monotonic and virtually linear over the all chain backbone. This is also the evidence for the almost perfectly stretched PEO chain backbone. Again, the small deviation at the free end is addressed to the flexibility enhancement at the edge of the brush.

In Figure 9, the distance of individual monomers from the siloxane surface reduced by the terminal-monomer distance,

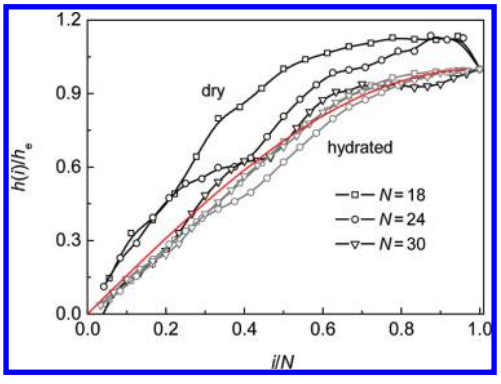

Figure 9. Average distance of the ith monomer from the siloxane surface reduced by the average distance of the end monomer plotted against the contour position of the ith monomer reduced by the number of monomers for PEO chains of lengths N grafted at the coverage densitiy σ = 1.092 nm^{-2}. The solid line represents the $\sin(i\pi/2N)$ function.

$h(i)/h_e$, is plotted against the relative monomer position along the chain backbone, i/N, in dry as well as in hydrated conditions. Such scaling enables straightforward comparison with the SCF predicted sinusoidal function sketched by the solid line in Figure 9. While at σ = 1.092 nm^{-2} the hydrated PEO chains generate swollen brushes, this is not true for the dry conditions. The curves for the hydrated PEO layers match the sinusoid function satisfactorily, but the curves for the dry PEO layers depart from the sinusoid function. Moreover, they do not coalesce into a single master curve. The maximum discussed above is also apparent here, and it approaches the sinusoid function from above. The same trend was established in another Monte Carlo study.[55]

3.4. Orientation Order Parameters. The orientation preference of bonds along the chain backbone under confinement induced by the grafting support can be deduced also from the first- and second-rank orientation order parameters defined as the first and second Legendre polynomials $\langle P_1(\cos\theta)\rangle$ and $\langle P_2(\cos\theta)\rangle$, respectively.

$$\langle P_1(\cos\theta)\rangle = \langle\cos\theta\rangle \quad (1)$$

$$\langle P_2(\cos\theta)\rangle = \frac{1}{2}(3\langle\cos^2\theta\rangle - 1) \quad (2)$$

The angular brackets stand for the averages over all conformations of all chains and θ denotes the angle between an effective bond and the surface normal. In the evaluation of the orientation order parameter, we consider as the effective bond $b_{i,i-1}$ a length scale incorporating the whole monomer unit $CH_2{}^{i-1}-CH_2-O-CH_2{}^{i}$ (indexing starts at the siloxane surface).

The orientation order parameters for different chain lengths and coverage densities are displayed in Figure 10. As one can

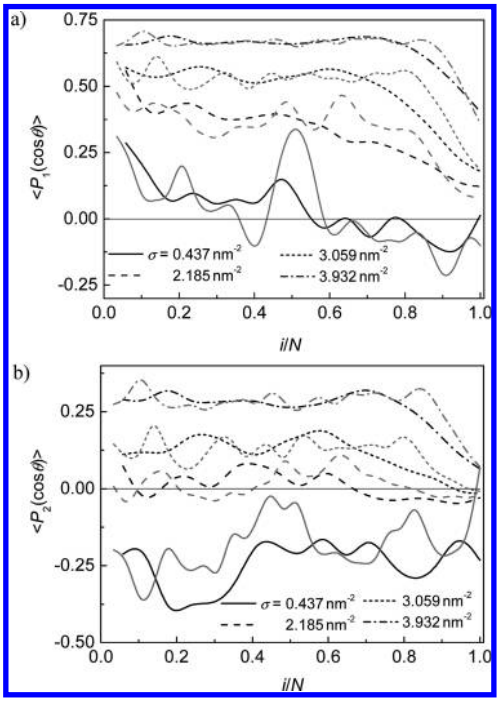

Figure 10. Dependence of the orientation order parameters of consecutive effective bonds $\langle P_1(\cos\theta)\rangle$ (a) and $\langle P_2(\cos\theta)\rangle$ (b) on the contour distance from the grafting points for PEO chains of N = 18 (black lines) and N = 30 (gray lines) grafted at coverage densities σ. The solid horizontal line intersecting y = 0 is a guide for the eye.

see, the chain lengths influence only marginally the trends of $\langle P_1(\cos\theta)\rangle$ (Figure 10a) and $\langle P_2(\cos\theta)\rangle$ (Figure 10b). However, the coverage densities do affect these parameters in a non-negligible way.

The intensive oscillations of $\langle P_1(\cos\theta)\rangle$ around a slightly declining line near the zero region for σ = 0.437 nm^{-2} demonstrate more or less disordered structure, and thus, they rule out the existence of the brush regime at this coverage density. The positive values of $\langle P_1(\cos\theta)\rangle$ in the inner region

dx.doi.org/10.1021/jp209802p | J. Phys. Chem. C 2012, 116, 3576−3584

of PEO layer turns to negative values in the outer region, while $\langle P_2(\cos\theta)\rangle$ fluctuates more or less around a constant, negative value. The former finding suggests that the outer segments of the chain backbones collapse into the inner region of the PEO layer as has been discussed above concerning Figure 8. The latter finding implies that the strong attraction between the monomers and the siloxane surface disfavors completely isotropic collapse, in which case $\langle P_2(\cos\theta)\rangle = 0$.

The plots of $\langle P_1(\cos\theta)\rangle$ for higher coverage densities exhibit similar trends with a broad flat initiation spreading over the larger portion of chains. The terminal drop-down is rather steep as a result of the more flexible chain end. With increasing σ values, the plateau broadens, and it is shifted upward along the y abscissa. The same trend is observed also for $\langle P_2(\cos\theta)\rangle$. The positive values of $\langle P_1(\cos\theta)\rangle$ and $\langle P_2(\cos\theta)\rangle$ reveal strongly stretched conformations of PEO chains without any back-folded patterns. The oscillations of $\langle P_2(\cos\theta)\rangle$ around zero value observed for PEO chains grafted at $\sigma = 2.185$ nm^{-2} indicate isotropic organization of the effective bonds. Since the corresponding $\langle P_1(\cos\theta)\rangle$ is positive, the brush should be weakly stretched at this coverage density. However, this does not contradict the findings of the previous work by Kuznetsov et al.,[56] according to which in poor-solvent conditions the grafted chains undergo transition from the isotropically to nematically collapsed state directly without any weakly stretched conformations. One should be aware that in the present simulations, the orientation of effective bonds is dictated not only by the coverage density but also by the attractive interactions with the siloxane surface.

For the highest coverage densities, even the terminal bonds exhibit a directional preference as it is recognized from the positive terminations of both order parameters. The plateau of $\langle P_2(\cos\theta)\rangle$ for $\sigma = 3.932$ nm^{-2} close to 0.3 gives a reason for suspecting the existence of a nematically ordered phase.[56] Conclusions drawn from Figure 10 are supported also by Figure 8. Besides, the plots in Figure 10 could be only qualitatively compared with theoretical estimates. The anticipated discrepancies may be due to the short chain length and specific interactions not accounted for in the theoretical analyses. We thus avoid drawing any quantitative comparison with the analytical results.

3.5. Two-Dimensional Radial Distribution Functions. The previous subsections point out that PEO chains grafted at higher coverage densities are characterized by a great deal of extension (Figure 8) and ordering over the large portion of the chain backbone (Figure 10), the characteristics that signify the presence of a nematic phase. In order to elucidate the phase behavior within the PEO layers, we have evaluated then the two-dimensional radial distribution functions (2D RDFs) around axes parallel to the z axis.

Figure 11 presents the normalized 2D RDFs for different coverage densities compared with 2D RDF of the bulk PEO system simulated in the *NPT* ensemble but in the same conditions otherwise. The positions of peaks in the RDFs are not affected by the chain length and at higher coverage densities, only the intensities at small r values are higher for longer chains. In Figure 11, the plots for grafted PEO chains of the contour length $N = 30$ are included, except for $\sigma = 0.437$ nm^{-2} in which case 2D RDF for $N = 18$ is plotted as well. Since at this coverage density, PEO chains experience relatively enhanced free space in the lateral dimensions, they are prone to merge the outer part of their backbone back into the anchored layer as it is demonstrated by the higher intensity of the first

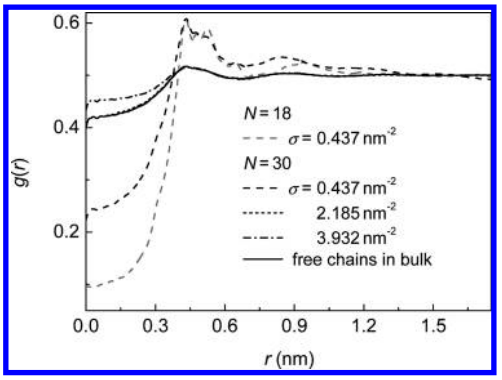

Figure 11. Normalized two-dimensional radial distribution function for grafted PEO chains of lengths N grafted at coverage densities σ.

peak. This nearest-neighbor peak is also richer in structuring; it is slightly more sensitive to the chain length, and it is identical with the first peak of the collapsed domain (Figure 1d) generated by PEO chains attached to the predominantly repulsive surface at $\sigma = 0.218$ nm^{-2} (not shown). All these findings support the above assertion of a collapsed compact conformation, deduced from the orientation order parameters.

With increasing coverage densities, the 2D RDFs become more flat and smooth resembling liquid phase. Interestingly, the 2D RDF for $\sigma = 2.185$ nm^{-2} tightly coincides with the 2D RDF of the bulk PEO chains of the same contour length. Seemingly, at this coverage density, the attractive effects of the siloxane surface on the orientation of effective bonds are compensated by the monomer repulsion due to their lateral overcrowding. This influence is also discernible in the second rank orientation order parameter discussed in the previous subsection.

Apart from $r < 0.3$ nm, the 2D RDFs for the higher coverage densities also fit the 2D RDF of the bulk system. This along with the absence of sharp peaks in the 2D RDFs highlights the liquid-like character of densely grafted PEO chains. The magnified intensity of the 2D RDFs at $r < 0.3$ nm for higher coverage densities are connected with a more vertical alignment of chains ensuing from the denser coverage of the siloxane surface. The coincidence of the 2D RDFs for grafted PEO chains with the 2D RDF of the bulk PEO system at $r > 0.3$ nm is linked with the increased flexibility of the chain backbone further from the grafting support, due to which they can fill the space by monomers similarly to the bulk.

We have also separately investigated the 2D RDF for $r > 0.3$ nm of the first and second half of grafted PEO chains to check if there were some crystalline domains formed from the inside of the chain as has been already observed.[57] Nevertheless, the 2D RDFs of both halves are identical.

4. CONCLUSIONS

In the present work, we have performed an atomistic MD study of structural properties of PEO chains irreversibly end-grafted on the siloxane surface in solvent-free conditions. We have focused on the detailed study of dry realistic polymer brushes at the all-atom level including specific interactions with the supporting surface. The main goal was to compare the obtained results with the analytic predictions. To the best of our knowledge, such a comparison has not been drawn yet. The coverage densities employed exceed the coverage densities commonly accessible in experimental setups. At very low coverage densities, the attractive interactions between EO monomers and siloxane atoms disallow generation of monomer

clusters that abundantly occur in poor-solvent conditions in the case of a repulsive grafting support. Instead, the chains generate two-dimensional crumpled structures adsorbed at the siloxane surface. However, upon switching the potential of the solid support to a more repulsive one, the chains aggregate into domains, thus forming a laterally inhomogeneous layer.

Although the initial structuring in the monomer distribution functions persists after removing water molecules, the respective peaks are more intensive, which stems from the enhanced compactness of EO monomers in the proximity of the siloxane surface. In comparison with the hydrated counterparts, the distributions become also more shrunken and abrupt before vanishing. In the brush regime, the plateaus are developed and well-correlated with the brush thickness. Even though a qualitative agreement with the SCF predictions of the solvent effect is achieved, one should notice that the characteristic structuring of monomer distributions in close vicinity of the solid support has not been predicted in the SCF theory.

Similarly, the chain-end density distributions of the dry PEO layers are also more contracted than the hydrated analogues, and the chain-ends are allowed to penetrate the siloxane layer. These distributions are getting narrower on increasing coverage density.

The linear dependence of brush height on both the chain length and coverage density predicted by the SCF theory is satisfactorily reproduced in our systems in spite of the relatively short backbones and attractive interactions between monomers and the siloxane support. The attractive effects of the siloxane support are gradually vanishing at $\sigma > 1.092$ nm^{-2}, and the chains become remarkably extended in the vertical direction.

The great deal of extension at higher coverage densities is corroborated also by the dependence of the distance of the individual monomer as a function of the monomer contour position, being thus linear along the majority of the whole chain backbone. The flexible terminal parts only slightly declines from a linear behavior. At lower coverage densities, the profiles display approximately a symmetric pattern as a consequence of the back-folding of the monomers more removed along the chain backbone from the grafting points. Nevertheless, the theoretically predicted dependence as being represented by sin $(i\pi/2N)$ is only found for the hydrated PEO brushes.

The overall orientation of the tethered PEO chains is determined by two opposite effects, the affinity of EO monomers for the siloxane support leading to contraction, and the lateral repulsion of monomers at sufficiently large coverage densities. While the later effects dominate the orientation at higher coverage densities, the former effects prevail at the less densely coated siloxane surface. The collapsed state at lower coverage densities is not isotropic because the siloxane plane induces a preferred orientation of the effective bonds, which yields $\langle P_2 (\cos \theta)\rangle < 0$. The mutual cancellation of both effects appears at $\sigma \approx 2.185$ nm^{-2}. At this coverage density, the chains turn out to display pronounced resemblance with the bulk PEO system. At higher coverage densities, the nematic liquid-like ordering of grafted PEO chains is observed without any indication of a crystalline phase.

■ ASSOCIATED CONTENT

Supporting Information

A scheme of the MD simulation full setup along with a table of all the nonbonded interaction potential parameters used. Two figures are shown additionally pertaining to the scaling of the gyration radius vs. the number of monomers in the grafted PEO chains (Figure S1) and the evolution of the interaction energy per one monomer with the coverage density of the grafted PEO chains (Figure S2). This material is available free of charge via the Internet at http://pubs.acs.org.

■ AUTHOR INFORMATION

Corresponding Author

*(Z.B.) Fax: +351 220402659. E-mail: upolzben@savba.sk. (M.N.D.S.C.) Fax: +351 220402659. E-mail: ncordeir@fc.up.pt.

Notes

The authors declare no competing financial interest.

■ ACKNOWLEDGMENTS

This work was supported by the FCT postdoc grant SFRH/BPD/63568/2009 cofinanced by the European Social Found. Moreover, this work was further supported by FCT through grant no. Pest-C/EQB/LA0006/2011. We also thank the Centre of Excellence Program of the Slovak Academy of Sciences (COMCHEM).

■ REFERENCES

(1) Milner, S. T.; Witten, T. A.; Cates, M. E. *Macromolecules* **1988**, *21*, 2610−2619.
(2) Milner, S. T.; Witten, T. A.; Cates, M. E. *Europhys. Lett.* **1988**, *5*, 413−418.
(3) Milner, S. T. *Science* **1991**, *251*, 905−914.
(4) Yu, Q.; Zhang, Y.; Chen, H.; Zhou, F.; Wu, Z.; Huang, H.; Brash, J. L. *Langmuir* **2010**, *26*, 8582−8588.
(5) Klein, J. *Annu. Rev. Mater. Sci.* **1996**, *26*, 581−612.
(6) Napper, D. H. *Polymeric Stabilization of Colloidal Dispersions*; Academic Press: London, U.K., 1983.
(7) Amiji, M.; Park, K. *J. Biomater. Sci., Polym. Ed.* **1993**, *4*, 217−234.
(8) Szleifer, I.; Carignano, M. A. *Macromol. Rapid Commun.* **1999**, *21*, 423−448.
(9) Alexander, S. *J. Phys.* **1977**, *38*, 983−987.
(10) de Gennes, P.-G. *Macromolecules* **1980**, *13*, 1069−1075.
(11) Grest, G. S.; Murat, M. *Macromolecules* **1989**, *22*, 4054−4059.
(12) Grest, G. S.; Murat, M. *Macromolecules* **1993**, *26*, 3108−3117.
(13) Grest, G. S. *Macromolecules* **1994**, *27*, 418−426.
(14) Chakrabarti, A.; Toral, R. *Macromolecules* **1990**, *23*, 2016−2021.
(15) Lai, P.-Y.; Binder, K. *J. Chem. Phys.* **1991**, *95*, 9288−9299.
(16) Chakrabarti, A. *J. Chem. Phys.* **1994**, *100*, 631−635.
(17) Karaiskos, E.; Bitsanis, I. A.; Anastasiadis, S. H. *J. Polym. Sci., Part B: Polym. Phys.* **2009**, *47*, 2449−2461.
(18) Pal, S.; Seidel, C. *Macromol. Theory Simul.* **2006**, *15*, 668−673.
(19) Binder, K.; Neelov, I. M. *Macromol. Theory Simul.* **1995**, *4*, 119−136.
(20) Watanabe, H.; Tirroll, M. *Macromolecules* **1993**, *26*, 6455−6466.
(21) Auroy, P.; Auvray, L.; Leger, L. *Macromolecules* **1991**, *24*, 2523−2528.
(22) Kent, M. S. *Macromol. Rapid Commun.* **2000**, *21*, 243−270.
(23) Sofia, S. J.; Premnath, V.; Merrill, E. W. *Macromolecules* **1998**, *31*, 5059−5070.
(24) Bedrov, D.; Smith, G. D. *Langmuir* **2006**, *22*, 6189−6194.
(25) Träskelin, P.; Kuhl, T. L.; Faller, R. *Phys. Chem. Chem. Phys.* **2009**, *11*, 11324−11332.
(26) Li, T.; Park, K. *Comput. Theory Polymer. Sci.* **2001**, *11*, 133−142.
(27) Duque, D.; Peterson, B. K.; Vega, L. F. *J. Phys. Chem. C* **2010**, *111*, 12328−12334.
(28) Roosjen, A.; van der Mei, H. C.; Busscher, H. J.; Norde, W. *Langmuir* **2004**, *20*, 10949−10955.
(29) Murthy, R.; Bailley, B. M.; Valentin-Rodriguez, C.; Ivanisevic, A.; Grunlan, M. A. *J. Polym. Sci., Part A: Polym. Chem.* **2010**, *48*, 4108−4119.

(30) McNamee, C. E.; Yamamoto, S.; Higashitani, K. *Langmuir* **2007**, *23*, 4389−4399.
(31) Piehler, J.; Brecht, A.; Valiokas, R.; Liedberg, B.; Gauglitz, G. *Biosens. Bioelectron.* **2000**, *15*, 473−481.
(32) Benková, Z.; Szefczyk, B.; D. S. Cordeiro, M. N. *Macromolecules* **2011**, *44*, 3639−3648.
(33) Maas, J. H.; Fleer, F. A.; Leermakers, F. A. M.; Cohen Stuart, M. A. *Langmuir* **2002**, *18*, 8871−8880.
(34) Holmes, P. F. *J. Biomed. Mater. Res., Part A* **2008**, *91*, 824−833.
(35) Siqueira, D. F.; Köhler, K.; Stamm, M. *Langmuir* **1995**, *11*, 3092−3096.
(36) Kwon, O.-H.; Ortalan, V.; Zewail, A. H. *Proc. Natl. Acad. Sci. U.S.A.* **2011**, *108*, 6026−6031.
(37) Zhu, X.-Y.; Jun, Y.; Staarup, D. R.; Major, R. C.; Danielson, S.; Boiadjiev, V.; Gladfelter, W. L.; Bunker, B. C.; Guo, A. *Langmuir* **2001**, *17*, 7798−7803.
(38) van der Spoel, D.; Lindahl, E.; Hess, B.; Groenhof, G.; Mark, A. E.; Berendsen, H. J. C. *J. Comput. Chem.* **2005**, *26*, 1701−1719.
(39) Hess, B.; van der Spoel, D.; Lindahl, E. *J. Chem. Theory Comput.* **2008**, *4*, 435−447.
(40) Vorobyov, I.; Anisimov, V. M.; Green, S.; Venable, R. M.; Moser, A.; Pastor, R. W.; MacKerell, A. D. J. *J. Chem. Theory Comput.* **2007**, *3*, 1120−1133.
(41) Lee, H.; Venable, R. M.; MacKerell, A. D.; Pastor, R. W. *Biophys. J.* **2008**, *95*, 1590−1599.
(42) Cruz-Chu, E. R.; Aksimentiev, A.; Schulten, K. *J. Phys. Chem. B* **2006**, *110*, 21497−21508.
(43) Parrinello, M.; Rahman, A. *J. Appl. Phys.* **1981**, *52*, 7182−7190.
(44) Nosé, S.; Klein, M. L. *Mol. Phys.* **1983**, *50*, 1055−1076.
(45) Nosé, S. *Mol. Phys.* **1984**, *52*, 255−268.
(46) Hoover, W. G. *Phys. Rev. A* **1985**, *31*, 1695−1697.
(47) Hess, B. *J. Chem. Theory Comput.* **2007**, *4*, 116−122.
(48) Darden, T.; York, D.; Pedersen, L. *J. Chem. Phys.* **1993**, *98*, 10089−10092.
(49) Essmann, U.; Perera, L.; Berkowitz, M. L.; Darden, T.; Lee, H.; Pedersen, L. *J. Chem. Phys.* **1995**, *103*, 8577−8592.
(50) Yeh, I.-C.; Berkowitz, M. L. *J. Chem. Phys.* **1999**, *111*, 3155−3162.
(51) Dimitrov, D. I.; Milchev, A.; Binder, K. *J. Chem. Phys.* **2007**, *127*, 084905.
(52) Benková, Z.; D. S. Cordeiro, M. N. *J. Phys. Chem. C* **2011**, *115*, 18740−18751.
(53) Zhulina, E. B.; Borisov, O. V.; Pryamitsyn, V. A.; Birshtein, T. M. *Macromolecules* **1991**, *24*, 140−149.
(54) *Aldrich Handbook of Fine Chemicals and Laboratory Equipment*; Aldrich Chemical Co.: Milwaukee, WI, 2004.
(55) Lai, P.-Y.; Binder, K. *J. Chem. Phys.* **1992**, *97*, 586−595.
(56) Kuznetsov, D. V.; Chen, Z. Y. *J. Chem. Phys.* **1998**, *109*, 7017−7027.
(57) He, G.-L.; Merlitz, H.; Sommer, J.-U.; Wu, C.-X. *Eur. Phys. J. E* **2007**, *24*, 325−330.